






# Delay-induced amplitude death in multiplex oscillator network with frequency-mismatched layers

メタデータ	言語: English 出版者: American Physical Society 公開日: 2024-08-28 キーワード (Ja): キーワード (En): 作成者: Konishi, Keiji, Yoshida, Koki, Sugitani, Yoshiki, Hara, Naoyuki メールアドレス: 所属:
URL	<a href="http://hdl.handle.net/10466/0002001148">http://hdl.handle.net/10466/0002001148</a>

## Delay-induced amplitude death in multiplex oscillator network with frequency-mismatched layers

Keiji Konishi <sup>1,\*</sup>, Koki Yoshida <sup>2</sup>, Yoshiaki Sugitani <sup>1</sup> and Naoyuki Hara<sup>1</sup>

<sup>1</sup>*Department of Electrical and Electronic Systems Engineering, Osaka Metropolitan University, 1-1 Gakuen-cho, Naka-ku, Sakai, Osaka 599-8531, Japan*

<sup>2</sup>*National Institute of Technology, Toyama College, 13 Hongo-machi, Toyama city, Toyama 939-8630, Japan*



(Received 2 September 2023; accepted 1 December 2023; published 19 January 2024)

The present paper analytically investigates the stability of amplitude death in a multiplex Stuart-Landau oscillator network with a delayed interlayer connection. The network consists of two frequency-mismatched layers, and all oscillators in each layer have identical frequencies. We show that, if the matrices describing the network topologies of each layer commute, then the characteristic equation governing the stability can be reduced to a simple form. This form reveals that the stability of amplitude death in the multiplex network is equally or more conservative than that in a pair of frequency-mismatched oscillators coupled by a delayed connection. In addition, we provide a procedure for designing the delayed interlayer connection such that amplitude death is stable for any commuting matrices and for any intralayer coupling strength. These analytical results are verified through numerical examples. Moreover, we numerically discuss the results for the case in which the commutative property does not hold.

DOI: [10.1103/PhysRevE.109.014220](https://doi.org/10.1103/PhysRevE.109.014220)

### I. INTRODUCTION

In past decades, considerable attention has been paid to collective phenomena in oscillators coupled by mutual interactions [1]. For example, cessation of oscillations has attracted a great deal of interest in the field of nonlinear science [2–13]. This phenomenon can be categorized as oscillation death or amplitude death according to its emergence property [9,10].

There has been growing interest in amplitude death [11,12] owing to its property that equilibrium points within oscillators are stabilized by mutual noninvasive interactions. This is because coupling signals, which realize the interactions, disappear after stabilization is complete. If the oscillators have a frequency mismatch, then diffusive coupling, the simplest noninvasive interaction, can induce amplitude death. However, if the oscillators do not have a frequency mismatch, then amplitude death is not induced [7,8]. In contrast, if the interactions involve time delays, then amplitude death can emerge even without a frequency mismatch [14–16]. Since for coupled oscillators in real situations, the propagation speed of coupling signals cannot be ignored, it is natural to consider delayed interactions. For this reason, numerous investigations on amplitude death induced by delayed coupling have been conducted from various viewpoints, such as modification of delayed coupling [17–23], application to thermoacoustic systems [24–30], and extension to oscillator networks [31–39].

Investigation of the stability of delay-induced amplitude death, which can promote its effective use in a wide range of applications, is in general not easy because the characteristic functions governing the stability are described by

quasipolynomial equations that have infinitely many roots. Fortunately, for oscillators without a frequency mismatch, the function can be analytically investigated. Several studies have conducted a stability analysis of delay-induced amplitude death [31–39]. In contrast, with a frequency mismatch, analytical investigations of stability become difficult. Quite recently, our previous study analytically investigated the stability with a frequency mismatch and clarified the mismatch effects on delay-induced amplitude death [40]. However, our study focused mainly on a pair of oscillators and extended the results only to oscillator networks with complete bipartite topologies [40]. Therefore, it is still a great challenge to extend the results with a frequency mismatch to oscillator networks with more general topologies.

Multiplex networks, a special type of multilayer network, have received broad attention from the viewpoint of network science [41,42]. In particular, in the field of nonlinear dynamics, there remains an increasing interest in the dynamical behavior of multiplex networks consisting of oscillators. Knowledge of various collective phenomena in multiplex oscillator networks, such as intralayer synchronizations [43–47], interlayer synchronizations [48–51], antiphase synchronizations [52,53], explosive synchronizations [54–57], and chimera states [58–65], has been accumulated. Furthermore, it has been reported that multiplexing can be used as a method for inducing or controlling stochastic resonance [66], self-induced stochastic resonance [67–69], and coherence resonance [68–71] in oscillator networks. Some of these reports use delay times in multiplexing networks and show that delay times play an important role for these resonances [67–69]. In addition to such reports, a great deal of effort has been devoted to the dynamics of oscillator networks coupled by delayed interlayer connections [72–80].

\*<https://www.omu.ac.jp/eng/ees-ecs>

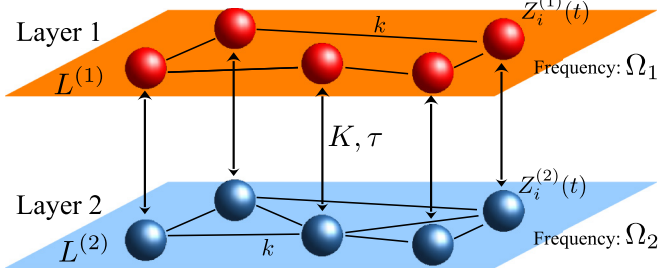


FIG. 1. Multiplex oscillator network with frequency mismatch.

As mentioned above, the dynamics of delay interlayer coupled networks is an attractive subject for study. However, to our knowledge, there have been few efforts to investigate amplitude death in such networks. The present study deals with amplitude death in a multiplex Stuart-Landau oscillator network with a delayed interlayer connection. This network consists of two frequency-mismatched layers, in which all oscillators in each layer have identical frequencies (see Fig. 1). The contribution of the present study is to analytically demonstrate the following: (1) If the matrices describing the network topologies of each layer commute, then the characteristic equation governing the stability of amplitude death can be reduced to a simple form. (2) The stability of amplitude death in a multiplex network is equally or more conservative than that in a pair of oscillators coupled by a delayed connection. (3) The analytical results of our previous study [40] can be used to design a delayed interlayer connection such that amplitude death is stable. These analytical findings are verified through some examples. In addition, numerical simulations suggest that these findings might be valid even if the commutative property does not hold.

The remainder of the present study is organized as follows. Section II presents the multiplex Stuart-Landau oscillator network with a delayed interlayer connection. In Sec. III, the main results of the present paper are analytically derived. In Sec. IV, the procedure for designing the delay time and the coupling strength of the interlayer connection is proposed. In Sec. V, for the case in which the commutative property does not hold, the procedure is numerically investigated, and the relationship with related previous studies is discussed.

## II. MULTIPLEX OSCILLATOR NETWORK

Let us consider a multiplex oscillator network with two frequency-mismatched layers (see Fig. 1),

$$\begin{aligned} \dot{Z}_i^{(1)}(t) = & F(Z_i^{(1)}(t), 0, \Omega_1) + K[Z_i^{(2)}(t - \tau) - Z_i^{(1)}(t)] \\ & + k \left[ \frac{1}{d_i^{(1)}} \left( \sum_{l=1}^N c_{il}^{(1)} Z_l^{(1)}(t) \right) - Z_i^{(1)}(t) \right], \end{aligned} \quad (1a)$$

$$\begin{aligned} \dot{Z}_i^{(2)}(t) = & F(Z_i^{(2)}(t), 0, \Omega_2) + K[Z_i^{(1)}(t - \tau) - Z_i^{(2)}(t)] \\ & + k \left[ \frac{1}{d_i^{(2)}} \left( \sum_{l=1}^N c_{il}^{(2)} Z_l^{(2)}(t) \right) - Z_i^{(2)}(t) \right]. \end{aligned} \quad (1b)$$

Here,  $F(Z, \mu, \Omega) := [1 - \mu + i\Omega - |Z|^2]Z$  describes the nonlinear dynamics of the Stuart-Landau oscillator, where

$i := \sqrt{-1}$  is the imaginary unit.  $Z_i^{(j)}(t) \in \mathbb{C}$  represents the state of oscillator  $i \in \{1, \dots, N\}$  at time  $t \geq 0$  in layer  $j \in \{1, 2\}$ , where  $N$  is the number of oscillators in each layer. The oscillators in layer  $j \in \{1, 2\}$  have a frequency of  $\Omega_j > 0$ ,

$$\Omega_1 := \bar{\Omega} + \frac{\Delta}{2}, \quad \Omega_2 := \bar{\Omega} - \frac{\Delta}{2}, \quad (2)$$

where  $\bar{\Omega} > 0$  is the nominal frequency, and  $\Delta \in [0, 2\bar{\Omega})$  is the frequency mismatch. In Eqs. (1a) and (1b), the second term on the right-hand side denotes the delayed interlayer coupling with delay time  $\tau \geq 0$  and coupling strength  $K \geq 0$ . The third term describes the no-delay intralayer coupling, where  $k \geq 0$  is the intralayer coupling strength. Here  $c_{il}^{(j)}$  represents the network topology in layer  $j$ : if oscillator  $i$  is connected to oscillator  $l$  in layer  $j$ , then  $c_{il}^{(j)} = c_{li}^{(j)} = 1$ , otherwise  $c_{il}^{(j)} = c_{li}^{(j)} = 0$ . For  $i = l$ , we have  $c_{ii}^{(j)} = 0$ . The degree of oscillator  $i$  in layer  $j$  is denoted by  $d_i^{(j)} := \sum_{l=1}^N c_{il}^{(j)} > 0$ .

The multiplex oscillator network (1) has the following equilibrium point:

$$Z_1^*(1) = \dots = Z_N^*(1) = Z_1^*(2) = \dots = Z_N^*(2) = 0. \quad (3)$$

The linearized dynamics of network (1) at point (3) is described by a time-delay linear system,

$$\dot{\mathbf{z}}(t) = \mathbf{A}_0 \mathbf{z}(t) + \mathbf{B} \mathbf{z}(t - \tau) - k \mathbf{A}_1 \mathbf{z}(t), \quad (4)$$

where its state variables,

$$\begin{aligned} \mathbf{z}(t) := & [z_1^{(1)}(t) \quad \dots \quad z_N^{(1)}(t) \quad z_1^{(2)}(t) \quad \dots \quad z_N^{(2)}(t)]^\top, \\ z_i^{(j)}(t) := & Z_i^{(j)}(t) - Z_i^*(j), \end{aligned} \quad (5)$$

denote small perturbations around point (3). The system matrices are given by

$$\begin{aligned} \mathbf{A}_0 := & \begin{bmatrix} (1 - K + i\Omega_1) \mathbf{I}_N & \mathbf{0} \\ \mathbf{0} & (1 - K + i\Omega_2) \mathbf{I}_N \end{bmatrix}, \\ \mathbf{A}_1 := & \begin{bmatrix} \mathbf{L}^{(1)} & \mathbf{0} \\ \mathbf{0} & \mathbf{L}^{(2)} \end{bmatrix}, \quad \mathbf{B} := \begin{bmatrix} \mathbf{0} & K \mathbf{I}_N \\ K \mathbf{I}_N & \mathbf{0} \end{bmatrix}, \end{aligned} \quad (6)$$

where  $\mathbf{L}^{(j)} := \mathbf{I}_N - \mathbf{C}^{(j)}$  represents the network topology in layer  $j$ . The elements of matrices  $\mathbf{C}^{(j)}$  are denoted as  $\{\mathbf{C}^{(j)}\}_{il} = c_{il}^{(j)}/d_i^{(j)}$  for  $i \neq l$  and  $\{\mathbf{C}^{(j)}\}_{il} = 0$  for  $i = l$ . The characteristic equation for system (4) is described as

$$\det[s\mathbf{I}_{2N} - \mathbf{A}_0 - \mathbf{B}e^{-s\tau} + k\mathbf{A}_1] = 0, \quad (7)$$

where  $s \in \mathbb{C}$  is the Laplace variable. Note that if  $\mathbf{L}^{(1)}$  and  $\mathbf{L}^{(2)}$  commute, then we have  $\Delta \mathbf{L} := \mathbf{L}^{(1)} \mathbf{L}^{(2)} - \mathbf{L}^{(2)} \mathbf{L}^{(1)} = \mathbf{0}$ .

## III. STABILITY ANALYSIS

This section analytically investigates the local stability of equilibrium point (3) on the basis of the characteristic equation (7). Since it is not easy to deal with Eq. (7) directly, under an assumption of topology, we simplify Eq. (7) as follows.

*Lemma 1.* Assume that  $\mathbf{L}^{(1)}$  and  $\mathbf{L}^{(2)}$  commute. Then, the characteristic equation (7) can be reduced to a simple form,

$$G(s) := \prod_{\ell=1}^N h(s, k\rho_{\ell}^{(1)}, k\rho_{\ell}^{(2)}) = 0, \quad (8)$$

$$h(s, \mu_1, \mu_2) := (s - 1 + \mu_1 + K - i\Omega_2) (s - 1 + \mu_2 + K - i\Omega_2) - K^2 e^{-2s\tau}, \quad (9)$$

where the eigenvalues of  $\mathbf{L}^{(1,2)}$  are denoted as  $\rho_{\ell}^{(1,2)}$  ( $\ell = 1, \dots, N$ ) and characterized by  $\mathbf{Q}^{-1}\mathbf{L}^{(1)}\mathbf{Q} = \text{diag}(\rho_1^{(1)}, \dots, \rho_N^{(1)})$  and  $\mathbf{Q}^{-1}\mathbf{L}^{(2)}\mathbf{Q} = \text{diag}(\rho_1^{(2)}, \dots, \rho_N^{(2)})$  with a common nonsingular matrix  $\mathbf{Q} \in \mathbb{R}^{N \times N}$ .

*Proof.* See Appendix A. ■

Lemma 1 indicates that the stability condition for equilibrium point (3) can be reduced to that of an equilibrium point for delay-coupled oscillators, as shown in the corollary below.

*Corollary 1.* Assume that  $\mathbf{L}^{(1)}$  and  $\mathbf{L}^{(2)}$  commute. The equilibrium point (3) for multiplex oscillator network (1) is locally stable if and only if the equilibrium point  $X_1^* = X_2^* = 0$  in delay-coupled oscillators with states  $X_{1,2}(t) \in \mathbb{C}$ ,

$$\begin{aligned} \dot{X}_1(t) &= F(X_1(t), k\rho_{\ell}^{(1)}, \Omega_1) + K\{X_2(t - \tau) - X_1(t)\} \\ \dot{X}_2(t) &= F(X_2(t), k\rho_{\ell}^{(2)}, \Omega_2) + K\{X_1(t - \tau) - X_2(t)\}, \end{aligned} \quad (10)$$

is locally stable for all  $\ell \in \{1, \dots, N\}$ .

*Proof.* See Appendix B. ■

Note that the eigenvalues of  $\mathbf{L}^{(1,2)}$  satisfy

$$\rho_{\ell}^{(1,2)} \in [0, 2], \quad \forall \ell \in \{1, \dots, N\}, \quad (11)$$

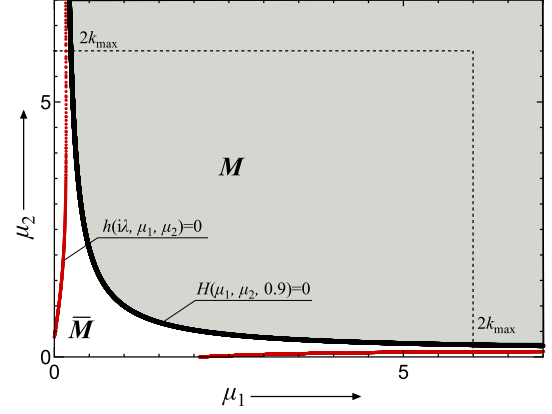
for any network topology [81,82]. Zero eigenvalues are always included in Eq. (11),

$$\rho_{\ell}^{(1,2)} = 0, \quad \exists \ell \in \{1, \dots, N\}, \quad (12)$$

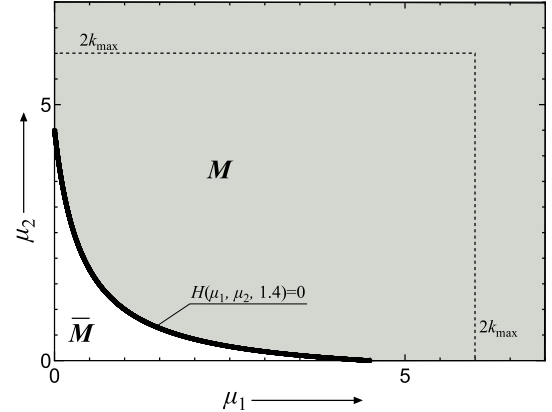
because  $\mathbf{L}^{(1,2)}$  have the eigenvector  $\mathbf{1}$  corresponding to zero eigenvalues. Since Eq. (12) holds, delay-coupled oscillators with  $\rho_{\ell}^{(1,2)} = 0$ ,

$$\begin{aligned} \dot{X}_1(t) &= F(X_1(t), 0, \Omega_1) + K\{X_2(t - \tau) - X_1(t)\} \\ \dot{X}_2(t) &= F(X_2(t), 0, \Omega_2) + K\{X_1(t - \tau) - X_2(t)\}, \end{aligned} \quad (13)$$

are always included in the set of delay-coupled oscillators (10) for  $\ell \in \{1, \dots, N\}$ . This inclusion indicates the following: the instability of  $X_1^* = X_2^* = 0$  in oscillators (13) is sufficient for point (3) in network (1) to be unstable; the stability of  $X_1^* = X_2^* = 0$  in oscillators (13) is necessary for point (3) to be stable. Note that oscillators (13) are frequency-mismatched oscillators coupled by a delayed connection considered in our previous work [40]. The instability can be represented by the following corollary.



(a) A:  $(\tau, K) = (0.3, 0.9)$



(b) B:  $(\tau, K) = (0.3, 1.4)$

FIG. 2. Sets of  $(\mu_1, \mu_2)$  satisfying  $H(\mu_1, \mu_2, K) = 0$  (solid black lines) and  $h(i\lambda, \mu_1, \mu_2) = 0$  (red lines) in  $(\mu_1, \mu_2)$  space: (a)  $(\tau, K) = (0.3, 0.9)$  and (b)  $(\tau, K) = (0.3, 1.4)$ .  $\mathbf{M}$  ( $\bar{\mathbf{M}}$ ) is the region over (under) the solid black line.

*Corollary 2.* If  $X_1^* = X_2^* = 0$  in delay-coupled oscillators (13) is unstable, then equilibrium point (3) for network (1) is never stabilized for any commuting  $\mathbf{L}^{(1,2)}$  or for any intralayer coupling strength  $k \geq 0$ .

This corollary shows that the stability condition for point (3) in network (1) is equally or more conservative than that for  $X_1^* = X_2^* = 0$  in oscillators (13). In other words, in the coupling parameter space  $(\tau, K)$ , the stability region for network (1) must be inside that for oscillators (13). Note that our previous study [40] analytically provides the boundary curves dividing stability and instability regions in space  $(\tau, K)$  for oscillators (13). Thus, with  $(\tau, K)$  in the instability region, amplitude death never occurs in network (1) for any commuting  $\mathbf{L}^{(1,2)}$  or for any  $k \geq 0$ . In addition, we see from  $h(s, 0, 0)$  that, in the case of no delay time ( $\tau = 0$ ) and no frequency mismatch ( $\Delta = 0$ ), amplitude death never occurs in network (1) for any commuting  $\mathbf{L}^{(1,2)}$ ,  $K \geq 0$ , or  $k \geq 0$ .

Let us consider the  $(\mu_1, \mu_2)$  space shown in Fig. 2(a) (in Fig. 2(b)) for  $K = 0.9 \in (1/2, 1]$  (for  $K = 1.4 > 1$ ). Note that, in what follows, we have to consider only the case of  $K > 1/2$  because  $X_1^* = X_2^* = 0$  in oscillators (13) is not

stabilized for any  $K \leq 1/2$  [40]. The solid black line represents the set of  $(\mu_1, \mu_2)$  satisfying  $H(\mu_1, \mu_2, K) = 0$ :

$$H(\mu_1, \mu_2, K) := |\mu_1 + K - 1| \cdot |\mu_2 + K - 1| - K^2. \quad (14)$$

The regions over and under the solid black line with  $\mu_{1,2} \geq 0$  are, respectively, defined by

$$\mathbf{M} := \{(\mu_1, \mu_2) \in \mathbb{R}_+^2 : H(\mu_1, \mu_2, K) > 0\}, \quad (15)$$

$$\overline{\mathbf{M}} := \{(\mu_1, \mu_2) \in \mathbb{R}_+^2 : H(\mu_1, \mu_2, K) \leq 0\}. \quad (16)$$

The gray (white) area in Fig. 2 represents  $\mathbf{M}$  ( $\overline{\mathbf{M}}$ ). Now, we provide a lemma on  $h(s, \mu_1, \mu_2)$  in Eq. (9) to support our main result.

*Lemma 2.* Roots  $s$  of  $h(s, \mu_1, \mu_2) = 0$  never intersect the imaginary axis for any  $(\mu_1, \mu_2) \in \mathbf{M}$ .

*Proof.* See Appendix C. ■

Lemma 2 is used to derive the following main result.

*Theorem 1.* The equilibrium point (3) for multiplex oscillator network (1) is locally stable for any commuting  $\mathbf{L}^{(1)}$  and  $\mathbf{L}^{(2)}$  and for any  $k \geq 0$ , if the following two conditions are satisfied:

- (a)  $(\tau, K)$  is chosen such that  $X_1^* = X_2^* = 0$  in oscillators (13) is locally stable [i.e.,  $h(s, 0, 0)$  is stable];
- (b) There does not exist  $\lambda \in \mathbb{R}$  for any  $(\mu_1, \mu_2) \in \overline{\mathbf{M}}$  such that  $h(i\lambda, \mu_1, \mu_2) = 0$  holds with the chosen  $(\tau, K)$ .

*Proof.* See Appendix D. ■

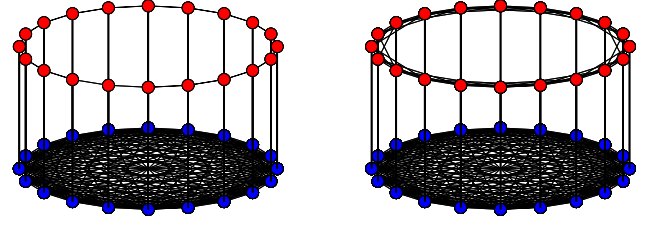
Condition (a) was easily realized in our previous study [40]. Condition (b) is numerically checked as to whether there exists  $\lambda \in \mathbb{R}$  in region  $\overline{\mathbf{M}}$ . Note that, for small  $K \in (1/2, 1]$ , region  $\overline{\mathbf{M}}$  becomes large [see Fig. 2(a)], which makes this region difficult to check numerically. In order to avoid such difficulty, we restrict the region by introducing the upper limit of the intralayer coupling strength  $k$  as follows.

*Corollary 3.* If the intralayer coupling strength is restricted to  $k \in [0, k_{\max})$ , where  $k_{\max}$  is the upper limit of the strength, then region  $\overline{\mathbf{M}}$  of condition (b) in Theorem 1 is replaced with

$$\overline{\mathbf{M}} := \{(\mu_1, \mu_2) \in \mathbb{R}_+^2 : H(\mu_1, \mu_2, K) \leq 0, \mu_{1,2} < 2k_{\max}\}. \quad (17)$$

*Proof.* See Appendix E. ■

Note that, for the case of  $\mathbf{L}^{(1)} = \mathbf{L}^{(2)}$ , condition (b) in Theorem 1 can be simplified (see Appendix F). The next section demonstrates Theorem 1 with Corollary 3 through numerical examples.



(a) Local ring and all-to-all layers

(b) Ring and all-to-all layers

FIG. 3. Multiplex oscillator networks consisting of commuting  $\mathbf{L}^{(1)}$  and  $\mathbf{L}^{(2)}$ : (a) local ring layer and all-to-all layer and (b) ring layer with three nearest neighbors in each direction and all-to-all layer.

#### IV. DESIGN OF $(\tau, K)$

In this section, based on Theorem 1 with Corollary 3, we design  $(\tau, K)$  such that equilibrium point (3) of multiplex oscillator network (1) is locally stable for any commuting  $\mathbf{L}^{(1)}$  and  $\mathbf{L}^{(2)}$  and for any  $k \in [0, k_{\max})$ . The procedure for designing  $(\tau, K)$  consists of the following steps:

- (1)  $(\tau, K)$  is designed for  $h(s, 0, 0)$  to be stable using our previous result [40] and  $k_{\max}$  is fixed;
- (2) Obtain  $(\lambda, \mu_1, \mu_2)$  satisfying  $h(i\lambda, \mu_1, \mu_2) = 0$  with the designed  $(\tau, K)$ ;
- (3) If the obtained  $(\mu_1, \mu_2)$  does not exist in  $\overline{\mathbf{M}}$  defined by Eq. (17), then the designed  $(\tau, K)$  satisfies Theorem 1 with Corollary 3.

It must be emphasized that if  $(\tau, K)$  is obtained through steps (1), (2), and (3), then point (3) of network (1) is locally stable for any commuting  $\mathbf{L}^{(1)}$  and  $\mathbf{L}^{(2)}$  and for any  $k \in [0, k_{\max})$ .

Let us numerically follow the procedure with  $(\overline{\Omega}, \Delta) = (10, 3.0)$ . For step (1), based on our previous result [40], we choose two sets: (A)  $(\tau, K) = (0.3, 0.9)$  and (B)  $(\tau, K) = (0.3, 1.4)$ . In addition,  $k_{\max} = 3$  is fixed. For step (2), we numerically obtain  $(\lambda, \mu_1, \mu_2)$  satisfying  $h(i\lambda, \mu_1, \mu_2) = 0$  using a software tool (e.g., MATLAB function `fimplicit`). The obtained data  $(\lambda, \mu_1, \mu_2)$  for sets (A) and (B) are, respectively, plotted as red curves on  $(\mu_1, \mu_2)$  space in Figs. 2(a) and 2(b). For step (3), we check whether there exist red lines  $(\mu_1, \mu_2)$  under black lines  $H(\mu_1, \mu_2, K) = 0$ . For set (A), there exist two red lines under the black line and within  $\mu_{1,2} \in [0, 6)$ . Thus, we see that set (A) does not satisfy Theorem 1 with Corollary 3. In contrast, for set (B), red lines do not exist. Set (B) satisfies the conditions in Theorem 1. As a conclusion, it is (is not) guaranteed that equilibrium point (3) for multiplex oscillator network (1) with (B)  $(\tau, K) = (0.3, 1.4)$  (with (A)  $(\tau, K) = (0.3, 0.9)$ ) is locally stable for any commuting  $\mathbf{L}^{(1)}$  and  $\mathbf{L}^{(2)}$  and for any  $k \in [0, 3)$ .

In order to confirm the conclusion obtained above, as an example, we use the multiplex oscillator networks (1) illustrated in Fig. 3. Now, we focus on the network with local ring layer  $\mathbf{L}^{(1)}$  and all-to-all layer  $\mathbf{L}^{(2)}$  [see Fig. 3(a)] for the cases of  $N = 15$  and  $N = 20$ . Note that  $\mathbf{L}^{(1)}$  and  $\mathbf{L}^{(2)}$  commute (i.e.,  $\Delta\mathbf{L} = \mathbf{0}$ ) independently of  $N$ . We use set (A)  $(\tau, K) = (0.3, 0.9)$ . Figure 4 is the enlarged illustration of Fig. 2(a). The thin lines passing through points  $\bullet$  represent  $(\mu_1, \mu_2) = (k\rho_\ell^{(1)}, k\rho_\ell^{(2)})$  ( $\ell = 1, \dots, N$ ) with  $N = 15$  for  $k \in [0, 3)$ . This is shown as follows. At  $k = 0$ ,  $(k\rho_\ell^{(1)}, k\rho_\ell^{(2)})$

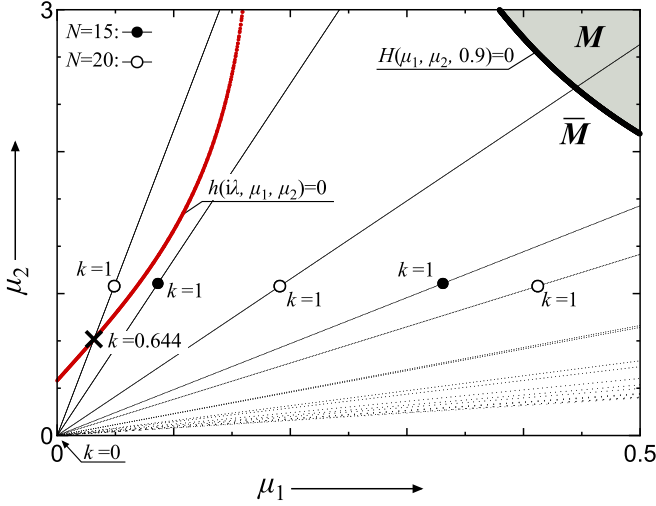


FIG. 4. Enlarged view of Fig. 2(a). The thin lines represent  $(\mu_1, \mu_2) = (k\rho_\ell^{(1)}, k\rho_\ell^{(2)})$  for  $k \in [0, 3)$ . The network consists of a local ring layer and an all-to-all layer with  $N = 15$  (•) and  $N = 20$  (◦).

( $\ell = 1, \dots, N$ ) are at the origin  $(0,0)$ , where all of the roots  $s \in \mathbb{C}$  of  $h(s, 0, 0) = 0$  are located in the open left-hand side of the complex plane owing to  $(\tau, K)$  chosen by condition (a) in Theorem 1, and  $(k\rho_\ell^{(1)}, k\rho_\ell^{(2)})$  ( $\ell = 1, \dots, N$ ) move from the origin to the top right as  $k$  increases from 0. At  $k = 1$ ,  $(k\rho_\ell^{(1)}, k\rho_\ell^{(2)})$  ( $\ell = 1, \dots, N$ ) reach points • representing eigenvalues  $(\rho_\ell^{(1)}, \rho_\ell^{(2)})$  of  $L^{(1)}$  and  $L^{(2)}$ , and  $(k\rho_\ell^{(1)}, k\rho_\ell^{(2)})$  ( $\ell = 1, \dots, N$ ) continue to move to the top right as  $k$  increases. We see that all  $(k\rho_\ell^{(1)}, k\rho_\ell^{(2)})$  ( $\ell = 1, \dots, N$ ) do not cross the red curve describing  $h(i\lambda, \mu_1, \mu_2) = 0$ . This indicates that, for  $N = 15$ , there does not exist  $\lambda \in \mathbb{R}$  for any  $(\mu_1, \mu_2) = (k\rho_\ell^{(1)}, k\rho_\ell^{(2)}) \in \bar{M}$  such that  $h(i\lambda, \mu_1, \mu_2) = 0$  holds with the chosen (A). In other words, every root  $s$  located in the open left-hand side at  $k = 0$  moves as  $k$  increases from 0 to 3, but never moves into the right-hand side.

For  $N = 20$ , the thin lines passing through points ◦ represent  $(\mu_1, \mu_2) = (k\rho_\ell^{(1)}, k\rho_\ell^{(2)})$  ( $\ell = 1, \dots, N$ ). As shown, one of the lines crosses the red curve at point  $\times$  with  $k = 0.644$ . This indicates that, for  $N = 20$ , there exists  $\lambda \in \mathbb{R}$  satisfying  $h(i\lambda, k\rho_\ell^{(1)}, k\rho_\ell^{(2)}) = 0$ . Therefore, as  $k$  increases from 0 to 3, at least one root  $s \in \mathbb{C}$  of  $h(s, \mu_1, \mu_2) = 0$  located in the open left-hand side at  $k = 0$  crosses the imaginary axis at  $k = 0.644$ , and then moves into the right-hand side. These results with  $N = 15$  and  $N = 20$  agree with the observation that, for (A)  $(\tau, K) = (0.3, 0.9)$ , it is not guaranteed that equilibrium point (3) is locally stable for any commuting  $L^{(1)}$  and  $L^{(2)}$  or for any  $k \in [0, 3)$ .

In contrast, for (B)  $(\tau, K) = (0.3, 1.4)$ , since red lines do not exist in Fig. 2(b), any root  $s$  located in the open left-hand side at  $k = 0$  does not cross the imaginary axis for any  $k \geq 0$ . This indicates that, for (B)  $(\tau, K) = (0.3, 1.4)$ , the stability is guaranteed for any commuting  $L^{(1)}$  and  $L^{(2)}$  and for any  $k \in [0, 3)$ . We consider the stability regions in  $(\tau, K)$  space (see Fig. 5), where the boundary curves for stability,  $\tau_{++}, \tau_{+-}, \tau_{-+}, \tau_{--}$  as denoted in our previous study [40], are drawn. Root  $s$  of  $h(s, 0, 0) = 0$ , which passes the imaginary axis at  $\tau = \tau_{++}, \tau_{--}$

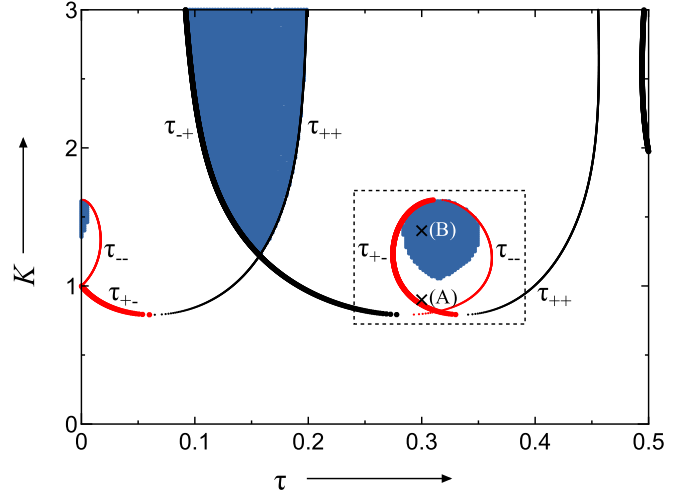


FIG. 5. Boundary curves for stability,  $\tau_{++}, \tau_{+-}, \tau_{-+}, \tau_{--}$  denoted in our previous study [40], in the coupling parameter space  $(\tau, K)$  and stability regions (blue areas) consisting of  $(\tau, K)$  obtained through steps (1), (2), and (3).

( $\tau_{+-}, \tau_{-+}$ ), moves from left (right) to right (left) with increasing  $\tau$ . The stability regions of  $h(s, 0, 0)$  are surrounded by a thick red line  $\tau_{+-}$  and a thin red line  $\tau_{--}$ , or by a thick black line  $\tau_{-+}$  and a thin black line  $\tau_{++}$ . In addition,  $(\tau, K)$  obtained through steps (1), (2), and (3) with  $k_{\max} = 3$  are plotted as blue points.<sup>1</sup> Note that if  $(\tau, K)$  is within the blue area, then point (3) of network (1) is locally stable for any commuting  $L^{(1)}$  and  $L^{(2)}$  and for any  $k \in [0, k_{\max})$ . Here, set (B) is in the blue area, but set (A) is not. This also agrees with the results in Fig. 2. Furthermore, Fig. 5 shows that the instability (stability) of  $X_1^* = X_2^* = 0$  in oscillators (13) is sufficient (necessary) for point (3) in network (1) to be unstable (stable). In addition, it is obvious that  $\bar{M}$  in step (3) shrinks with decreasing  $k_{\max}$  due to Eq. (17); this shrinking increases the possibility of  $(\tau, K)$  passing through step (3). As a result, the blue area never becomes smaller with decreasing  $k_{\max}$ .

Let us focus on the dotted box in Fig. 5. An enlarged view of the box region is shown in Fig. 6(a). Now we compare the stability region (blue area) with the stability regions (gray areas) that are numerically obtained by solving Eq. (7) at  $k = 1$  (see Appendix G). Figures 6(b) and 6(c) show the regions<sup>2</sup> with  $N = 15$  and 20, respectively, for the network shown in Fig. 3(a). The stability region with  $N = 15$  in Fig. 6(b) includes the blue area in Fig. 6(a) and set (A). For  $N = 20$ , the region in Fig. 6(c) shrinks and does not include set (A). These findings for  $N = 15$  and 20 agree with the results shown in Figs. 2 and 4. Figure 6(d) shows the stability region for the network of Fig. 3(b). The network consists of a ring layer with

<sup>1</sup> $(\tau, K)$  are set in  $200 \times 200$  grids with  $\tau \in [0.0, 0.5]$  and  $K \in [0.0, 3.0]$ . A blue point is plotted if  $(\tau, K)$  passes through all the steps.

<sup>2</sup> $(\tau, K)$  are set in  $200 \times 200$  grids with  $\tau \in [0.25, 0.40]$  and  $K \in [0.5, 2.0]$ . Gray points are plotted if the rightmost root of the characteristic equation for the real state system (G1) (see Appendix G) on the grids has a negative real part.

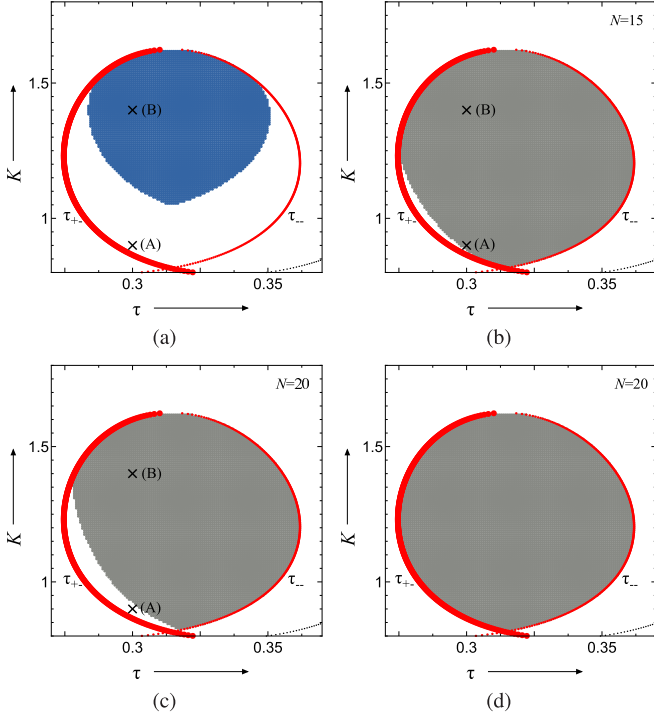


FIG. 6. Boundary curves for stability,  $\tau_{+,--}$ , in coupling parameter space  $(\tau, K)$  and stability regions. (a) Stability region (blue area) obtained through steps (1), (2), and (3). (b, c) Stability regions (gray areas) obtained in Appendix G for the network with local ring layer and all-to-all layer shown in Fig. 3(a) for (b)  $N = 15$  and (c)  $N = 20$ . (d) Stability region (gray area) with ring layer with three nearest neighbors in each direction and all-to-all layer of Fig. 3(b) for  $N = 20$ .

three nearest neighbors in each direction and an all-to-all layer ( $N = 20$ ), where  $\mathbf{L}^{(1)}$  and  $\mathbf{L}^{(2)}$  commute (i.e.,  $\Delta\mathbf{L} = \mathbf{0}$ ). The region fits that for  $h(s, 0, 0)$  even for  $N = 20$ . These results numerically support the finding that the stability region for network (1) is inside that for oscillators (13). The stability condition for point (3) in network (1) is equally or more conservative than that of  $X_1^* = X_2^* = 0$  in oscillators (13).

The main results of this section are summarized below. Under the assumption that  $\mathbf{L}^{(1)}$  and  $\mathbf{L}^{(2)}$  commute and  $k$  is restricted to  $k \in [0, k_{\max})$ , the stability regions (blue areas) obtained by the proposed procedure are valid independently of the commuting  $\mathbf{L}^{(1,2)}$ , the intralayer coupling strength  $k \in [0, k_{\max})$ , and the number of oscillators,  $N$ . This result is an advantage in the following situations: (1) information on the network topology, the number of oscillators, or the intralayer coupling strength is unknown, (2) information in situation (1) is often changed, and (3) the number of oscillators is large. For situation (1), characteristic equation (7) is not obtained; hence, it is quite difficult to numerically check the stability. For situation (2), even if information can be obtained in advance, it is necessary to numerically estimate the stability region of Eq. (7) using Appendix G every time information is changed. For situation (3), the dimensions of matrices,  $\mathbf{A}_0$ ,  $\mathbf{A}_1$ , and  $\mathbf{B}$ , in Eq. (7) are large; thus, the computation load in estimating the stability regions is heavy. It should be noted that even for such situations, the proposed procedure allows us to obtain the

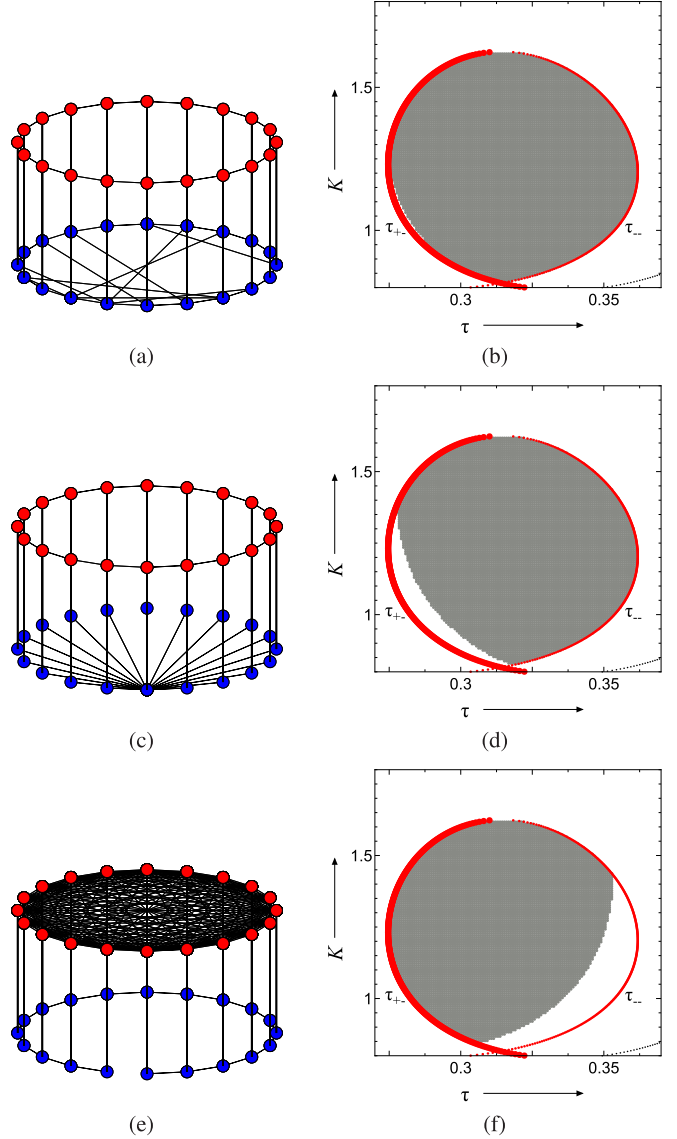


FIG. 7. Multiplex oscillator network with noncommuting  $\mathbf{L}^{(1)}$  and  $\mathbf{L}^{(2)}$ , boundary curves  $\tau_{+,--}$ , and stability regions (gray areas) obtained with Appendix G for  $N = 20$  and  $k = 1$ : (a, b) local ring layer and local ring layer with ten additional random shortcuts, (c, d) local ring layer and star layer, and (e, f) all-to-all layer and chain layer.

stability regions without a heavy computation load. We can therefore conclude that, for network (1) with the commutative property, the proposed procedure offers more versatility than conventional procedures.

## V. DISCUSSION

In this section, with some examples, we numerically investigate the case of noncommuting  $\mathbf{L}^{(1)}$  and  $\mathbf{L}^{(2)}$ . Furthermore, we discuss previous studies related to the present study.

For the case of noncommuting  $\mathbf{L}^{(1)}$  and  $\mathbf{L}^{(2)}$ , we consider three examples, where  $N = 20$  and  $k = 1$  are fixed (see Fig. 7). For the first example illustrated in Fig. 7(a), layer 1 has a local ring topology and layer 2 has a local ring topology with

ten additional random shortcuts. Here,  $L^{(1)}$  and  $L^{(2)}$  do not commute (i.e.,  $\|\Delta L\|_2 = 0.6148$ ). Thus, the analytical results obtained in Secs. III and IV cannot be used. Figure 7(b) shows, in  $(\tau, K)$  space, the stability parameter set that is numerically obtained by solving Eq. (7) with Appendix G<sup>3</sup> is slightly smaller than the stability region surrounded by the boundary curves  $\tau_{+,-,-}$  (red lines). For the second example, layers 1 and 2 have local ring and star topologies, respectively, as shown in Fig. 7(c) ( $\|\Delta L\|_2 = 5.2440$ ). The stability parameter set in Fig. 7(d) is smaller than the stability region. For the third example, as shown in Fig. 7(e), layers 1 and 2, respectively, have an all-to-all topology and a chain topology ( $\|\Delta L\|_2 = 0.2354$ ). Figure 7(f) shows that the stability parameter set is also smaller than the stability region. These examples show that, even with noncommuting  $L^{(1)}$  and  $L^{(2)}$ , the stability parameter set (gray area) is inside the stability region surrounded by the boundary curves and contains the stability region (blue area) in Fig. 6(a). These results appear to be the same as those obtained with commuting  $L^{(1)}$  and  $L^{(2)}$ . Thus, our analytical results might be useful in the case of noncommuting  $L^{(1)}$  and  $L^{(2)}$ . However, this is not analytically guaranteed.

Here, we briefly review three previous studies related to the present study. For the case in which the network topology in layers 1 and 2 are identical, networks (1) are categorized into a particular class of Cartesian product networks of delay-coupled oscillators, as denoted in a previous study [83], in which a procedure for designing the coupling parameters inducing amplitude death is provided. The previous study [83] treated time-delay mismatch, but not frequency mismatch. Recently, it was reported that various phenomena, including amplitude death, occur on multiplex networks consisting of Hindmarsh-Rose neuron models [84], and amplitude death occurs on multiplex Stuart-Landau oscillator networks with both attractive and repulsive connections [85]. However, these studies did not treat the delayed interlayer coupling focused on in the present study.

## VI. CONCLUSIONS

In the present paper, we have investigated the stability of amplitude death in a delay interlayer coupled multiplex Stuart-Landau oscillator network with two frequency-mismatched layers. It was analytically revealed that the characteristic equation governing the stability can be simplified if the matrices describing the topologies of each layer commute. The simplified equation clarified that the stability of amplitude death in the multiplex network is equally or more conservative than that in a pair of frequency-mismatched oscillators coupled by a delayed connection. Based on our previous study [40], we provided a procedure consisting of the three steps for designing the delayed interlayer connection such that amplitude death is stable for any commuting matrices and for any intralayer coupling strength. Furthermore, we discussed the results for the case in which the commutative property does not hold.

<sup>3</sup>The numerical procedure is the same as that for Figs. 6(b), 6(c), and 6(d).

## ACKNOWLEDGMENTS

The present study was supported in part by JSPS KAKENHI (Grants No. JP21H03513 and No. JP23K11245).

## APPENDIX A: PROOF OF LEMMA 1

If the matrices  $L^{(1)}$  and  $L^{(2)}$  commute (i.e.,  $L^{(1)}L^{(2)} = L^{(2)}L^{(1)}$ ), then there exists a common nonsingular matrix  $Q \in \mathbb{R}^{N \times N}$  such that  $Q^{-1}L^{(1)}Q = \text{diag}(\rho_1^{(1)}, \dots, \rho_N^{(1)})$  and  $Q^{-1}L^{(2)}Q = \text{diag}(\rho_1^{(2)}, \dots, \rho_N^{(2)})$  hold [86]. By introducing  $\det[I_2 \otimes Q^{-1}]$  and  $\det[I_2 \otimes Q]$ , Eq. (7) can be rewritten as

$$\det \begin{bmatrix} h(s, k\rho_1^{(1)}, k\rho_1^{(2)}) & \cdots & 0 \\ \vdots & \ddots & \vdots \\ 0 & \cdots & h(s, k\rho_N^{(1)}, k\rho_N^{(2)}) \end{bmatrix} = 0. \quad (\text{A1})$$

Thus, Eq. (A1) is equivalent to Eq. (8).

## APPENDIX B: PROOF OF COROLLARY 1

Lemma 1 shows that the local stability of equilibrium point (3) is governed by  $G(s) = 0$  that depends on eigenvalues  $\rho_\ell^{(1,2)}$  ( $\ell = 1, \dots, N$ ). Then  $h(s, k\rho_\ell^{(1)}, k\rho_\ell^{(2)})$  is the characteristic function for delay-coupled oscillators (10) at  $X_1^* = X_2^* = 0$ . Function  $G(s)$  is the product of  $h(s, k\rho_\ell^{(1)}, k\rho_\ell^{(2)})$  ( $\ell = 1, \dots, N$ ). Thus, the stability of  $G(s)$  is equivalent to the local stability of  $X_1^* = X_2^* = 0$  in delay-coupled oscillators (10) for all  $\ell \in \{1, \dots, N\}$ .

## APPENDIX C: PROOF OF LEMMA 2

If the roots  $s$  of  $h(s, \mu_1, \mu_2) = 0$  intersect the imaginary axis with some  $(\mu_1, \mu_2) \in \mathbf{M}$ , then at least one  $\lambda \in \mathbb{R}$  of  $h(i\lambda, \mu_1, \mu_2) = 0$  exists. In other words, if there does not exist  $\lambda \in \mathbb{R}$  satisfying  $h(i\lambda, \mu_1, \mu_2) = 0$  for any  $(\mu_1, \mu_2) \in \mathbf{M}$ , then the roots never intersect the imaginary axis for any  $(\mu_1, \mu_2) \in \mathbf{M}$ . Here  $h(i\lambda, \mu_1, \mu_2) = 0$  can be rewritten as

$$[\mu_1 + K - 1 - i(\Omega_1 - \lambda)][\mu_2 + K - 1 - i(\Omega_2 - \lambda)] = K^2 e^{-i2\lambda\tau}. \quad (\text{C1})$$

From the viewpoint of polar coordinates, we see that the modulus of the right-hand side of Eq. (C1) is  $K^2$ . It is clear that both the first and second factors on the left-hand side have moduli equal to or larger than  $|\mu_1 + K - 1|$  and  $|\mu_2 + K - 1|$ , respectively, for any  $\lambda \in \mathbb{R}$ . This fact guarantees that, if  $H(\mu_1, \mu_2, K) > 0$  holds, then Eq. (C1) does not hold for any  $\lambda \in \mathbb{R}$ . It is easy to see that  $(\mu_1, \mu_2)$  satisfying  $H(\mu_1, \mu_2, K) > 0$  are described by the region  $\mathbf{M}$ . As a result, roots  $s$  of  $h(s, \mu_1, \mu_2) = 0$  never intersect the imaginary axis for any  $(\mu_1, \mu_2) \in \mathbf{M}$ .

## APPENDIX D: PROOF OF THEOREM 1

Lemma 1 indicates that the local stability of equilibrium point (3) is equivalent to that of  $h(s, k\rho_\ell^{(1)}, k\rho_\ell^{(2)})$  for all  $\ell \in \{1, \dots, N\}$ . Here  $k \geq 0$  holds, and  $\rho_\ell^{(1,2)}$  are restricted by Eqs. (11) and (12). Thus, if  $h(s, \mu_1, \mu_2)$  is stable for all  $(\mu_1, \mu_2) \in \mathbb{R}_+^2$ , then equilibrium point (3) is locally stable



for any  $k \geq 0$  and for any commuting  $\mathbf{L}^{(1)}$  and  $\mathbf{L}^{(2)}$ . In what follows, we will focus on the stability of  $h(s, \mu_1, \mu_2)$  for  $(\mu_1, \mu_2) = (0, 0)$ , for  $(\mu_1, \mu_2) \in \overline{\mathbf{M}}$ , and for  $(\mu_1, \mu_2) \in \mathbf{M}$ . For  $(\mu_1, \mu_2) = (0, 0)$ , if condition (a) holds, all roots  $s$  of  $h(s, 0, 0) = 0$  are located in the open left-hand side of the complex plane. For any  $(\mu_1, \mu_2) \in \overline{\mathbf{M}}$ , if condition (b) holds, then none of the roots ever intersect the imaginary axis. For any  $(\mu_1, \mu_2) \in \mathbf{M}$ , Lemma 2 shows that none of the roots ever intersect the imaginary axis. As a result, if conditions (a) and (b) are satisfied, then the roots  $s$  of  $h(s, 0, 0) = 0$  located in the open left-hand side never intersect the imaginary axis for any  $(\mu_1, \mu_2) \in \mathbb{R}_+^2$  (i.e.,  $h(s, \mu_1, \mu_2)$  is stable for any  $(\mu_1, \mu_2) \in \mathbb{R}_+^2$ ).

### APPENDIX E: PROOF OF COROLLARY 3

Since the upper limit of the eigenvalues  $\rho_\ell^{(1,2)}$  is 2, the upper limit of  $k\rho_\ell^{(1,2)}$  is  $2k_{\max}$ . Thus, it is sufficient for us to consider the region defined by Eq. (17) rather than that defined by Eq. (16).

### APPENDIX F: CASE OF $\mathbf{L}^{(1)} = \mathbf{L}^{(2)}$

Consider our results in Theorem 1 for the case in which the network topologies in layers 1 and 2 are identical (that is,  $\mathbf{L}^{(1)} = \mathbf{L}^{(2)}$  holds). Their eigenvalues are equivalent,  $\rho_\ell^{(1)} = \rho_\ell^{(2)} \in [0, 2]$  for all  $\ell \in \{1, \dots, N\}$ . Region  $\overline{\mathbf{M}}$  shrinks to line  $\mu = \mu_1 = \mu_2 \in [0, 1]$  in  $(\mu_1, \mu_2)$  space. Therefore, condition (b) in Theorem 1 can be simplified as follows.

There does not exist  $\lambda \in \mathbb{R}$  for any  $\mu \in [0, 1]$  such that  $h(i\lambda, \mu, \mu) = 0$  holds with the chosen  $(\tau, K)$ .

### APPENDIX G: SYSTEM (4) WITH REAL STATE VARIABLES

The time-delay linear system (4) with complex state variables can be rewritten as

$$\begin{aligned} \dot{\hat{\mathbf{z}}}(t) &= \hat{\mathbf{A}}_0 \hat{\mathbf{z}}(t) + \hat{\mathbf{B}} \hat{\mathbf{z}}(t - \tau) - k \hat{\mathbf{A}}_1 \hat{\mathbf{z}}(t), \quad (\text{G1}) \\ \hat{\mathbf{A}}_0 &:= \begin{bmatrix} (1-K)\mathbf{I}_N & -\Omega_1 \mathbf{I}_N & \mathbf{0} & \mathbf{0} \\ \Omega_1 \mathbf{I}_N & (1-K)\mathbf{I}_N & \mathbf{0} & \mathbf{0} \\ \mathbf{0} & \mathbf{0} & (1-K)\mathbf{I}_N & -\Omega_2 \mathbf{I}_N \\ \mathbf{0} & \mathbf{0} & \Omega_2 \mathbf{I}_N & (1-K)\mathbf{I}_N \end{bmatrix}, \\ \hat{\mathbf{A}}_1 &:= \text{diag}(\mathbf{L}^{(1)}, \mathbf{L}^{(1)}, \mathbf{L}^{(2)}, \mathbf{L}^{(2)}), \quad \hat{\mathbf{B}} := \begin{bmatrix} \mathbf{0} & \mathbf{I}_2 \\ \mathbf{I}_2 & \mathbf{0} \end{bmatrix} \otimes K \mathbf{I}_N, \quad (\text{G2}) \end{aligned}$$

with real state variables,

$$\begin{aligned} \hat{\mathbf{z}}(t) &:= \begin{bmatrix} \text{Re}(\mathbf{z}^{(1)}(t))^\top & \text{Im}(\mathbf{z}^{(1)}(t))^\top & \text{Re}(\mathbf{z}^{(2)}(t))^\top \\ & & \text{Im}(\mathbf{z}^{(2)}(t))^\top \end{bmatrix}^\top, \quad (\text{G3}) \end{aligned}$$

where  $\mathbf{z}^{(j)}(t) := [z_1^{(j)}(t) \ \dots \ z_N^{(j)}(t)]^\top$ ,  $j \in \{1, 2\}$ . The roots of the characteristic equation for the real state system (G1) can be numerically found using the software tool eigAM [87].

- 
- [1] S. Boccaletti, A. N. Pisarchik, C. I. del Genio, and A. Amann, *Synchronization* (Cambridge University Press, Cambridge, 2018).
- [2] Y. Yamaguchi and H. Shimizu, *Physica D* **11**, 212 (1984).
- [3] K. Bar-Eli, *Physica D* **14**, 242 (1985).
- [4] G. Ermentrout and W. Troy, *SIAM J. Appl. Math.* **46**, 359 (1986).
- [5] H. Sakaguchi, *Prog. Theor. Phys.* **80**, 743 (1988).
- [6] M. Shiino and M. Frankowicz, *Phys. Lett. A* **136**, 103 (1989).
- [7] R. E. Mirollo and S. H. Strogatz, *J. Stat. Phys.* **60**, 245 (1990).
- [8] D. G. Aronson, G. B. Ermentrout, and N. Kopell, *Physica D* **41**, 403 (1990).
- [9] G. Saxena, A. Prasad, and R. Ramaswamy, *Phys. Rep.* **521**, 205 (2012).
- [10] A. Koseska, E. Volkov, and J. Kurths, *Phys. Rep.* **531**, 173 (2013).
- [11] Y. Sugitani and K. Konishi, *Nonlinear Theor. Appl., IEICE* **12**, 612 (2021).
- [12] W. Zou, D. V. Senthilkumar, M. Zhan, and J. Kurths, *Phys. Rep.* **931**, 1 (2021).
- [13] W. Zou, S. He, D. V. Senthilkumar, and J. Kurths, *Phys. Rev. Lett.* **130**, 107202 (2023).
- [14] D. V. Ramana Reddy, A. Sen, and G. L. Johnston, *Phys. Rev. Lett.* **80**, 5109 (1998).
- [15] D. V. Ramana Reddy, A. Sen, and G. L. Johnston, *Physica D* **129**, 15 (1999).
- [16] D. V. Ramana Reddy, A. Sen, and G. L. Johnston, *Phys. Rev. Lett.* **85**, 3381 (2000).
- [17] W. Zou, Y. Tang, L. Li, and J. Kurths, *Phys. Rev. E* **85**, 046206 (2012).
- [18] Y. N. Kyrychko, K. B. Blyuss, and E. Schöll, *Philos. Trans. R. Soc. A* **371**, 20120466 (2013).
- [19] Y. Sugitani, K. Konishi, and N. Hara, *Phys. Rev. E* **92**, 042928 (2015).
- [20] R. M. Nguimdo, *Phys. Rev. E* **97**, 032211 (2018).
- [21] A. Otto, G. Radons, D. Bachrathy, and G. Orosz, *Phys. Rev. E* **97**, 012311 (2018).
- [22] A. Sharma, *Phys. Lett. A* **383**, 1865 (2019).
- [23] A. Ghosh, S. Mondal, and R. I. Sujith, *Chaos* **32**, 101106 (2022).
- [24] R. I. Sujith and S. A. Pawar, *Thermoacoustic Instability* (Springer, Cham, 2021).
- [25] T. Biwa, S. Tozuka, and T. Yazaki, *Phys. Rev. Appl.* **3**, 034006 (2015).
- [26] K. Moon, Y. Guan, L. K. B. Li, and K. T. Kim, *Chaos* **30**, 023110 (2020).
- [27] H. Hyodo, M. Iwasaki, and T. Biwa, *J. Appl. Phys.* **128**, 094902 (2020).
- [28] D. Premraj, K. Manoj, S. A. Pawar, and R. I. Sujith, *Nonlinear Dyn.* **103**, 1439 (2021).
- [29] M. H. Doranehgard, V. Gupta, and L. K. B. Li, *Phys. Rev. E* **105**, 064206 (2022).
- [30] S. Srikanth, S. A. Pawar, K. Manoj, and R. I. Sujith, *Chaos* **32**, 073129 (2022).

- [31] R. Dodla, A. Sen, and G. L. Johnston, *Phys. Rev. E* **69**, 056217 (2004).
- [32] M. P. Mehta and A. Sen, *Phys. Lett. A* **355**, 202 (2006).
- [33] Y. Sugitani, K. Konishi, L. B. Le, and N. Hara, *Chaos* **24**, 043105 (2014).
- [34] S. R. Huddy and J. Sun, *Phys. Rev. E* **93**, 052209 (2016).
- [35] S. R. Huddy, *Chaos* **30**, 013118 (2020).
- [36] Y. Okigawa, Y. Sugitani, and K. Konishi, *Eur. Phys. J. B* **93**, 129 (2020).
- [37] N. Zhao and Z. Sun, *Int. J. Bifurcation Chaos* **30**, 2050094 (2020).
- [38] Y. Sugitani and K. Konishi, *Phys. Rev. E* **105**, 064202 (2022).
- [39] W. Zou, Y. Chen, D. V. Senthilkumar, and J. Kurths, *Chaos* **32**, 041102 (2022).
- [40] S. Mizukami, K. Konishi, Y. Sugitani, T. Kouda, and N. Hara, *Phys. Rev. E* **104**, 054207 (2021).
- [41] G. Bianconi, *Multilayer Networks* (Oxford University Press, Oxford, 2018).
- [42] R. Berner, V. Mehrmann, E. Schöll, and S. Yanchuk, *SIAM J. Appl. Dyn. Syst.* **20**, 1752 (2021).
- [43] L. V. Gambuzza, M. Frasca, and J. Gómez-Gardeñes, *Europhys. Lett.* **110**, 20010 (2015).
- [44] B. K. Bera, S. Rakshit, and D. Ghosh, *Eur. Phys. J.: Spec. Top.* **228**, 2441 (2019).
- [45] S. Rakshit, B. K. Bera, E. M. Bollt, and D. Ghosh, *SIAM J. Appl. Dyn. Syst.* **19**, 918 (2020).
- [46] L. Tang, X. Wu, J. Lü, J. A. Lu, and R. M. D'Souza, *Phys. Rev. E* **99**, 012304 (2019).
- [47] M. S. Anwar and D. Ghosh, *Chaos* **32**, 033125 (2022).
- [48] R. Sevilla-Escoboza, I. Sendiña-Nadal, I. Leyva, R. Gutiérrez, J. M. Buldú, and S. Boccaletti, *Chaos* **26**, 065304 (2016).
- [49] I. Leyva, R. Sevilla-Escoboza, I. Sendiña-Nadal, R. Gutiérrez, J. Buldú, and S. Boccaletti, *Sci. Rep.* **7**, 45475 (2017).
- [50] S. Rakshit, B. K. Bera, and D. Ghosh, *Phys. Rev. E* **101**, 012308 (2020).
- [51] S. Nag Chowdhury, S. Rakshit, C. Hens, and D. Ghosh, *Phys. Rev. E* **107**, 034313 (2023).
- [52] S. N. Chowdhury, S. Rakshit, J. M. Buldú, D. Ghosh, and C. Hens, *Phys. Rev. E* **103**, 032310 (2021).
- [53] I. Shepelev, A. Bukh, and G. Strelkova, *Chaos Solitons Fractals* **162**, 112447 (2022).
- [54] P. Khanra, P. Kundu, C. Hens, and P. Pal, *Phys. Rev. E* **98**, 052315 (2018).
- [55] A. D. Kachhvah and S. Jalan, *New J. Phys.* **21**, 015006 (2019).
- [56] S. Jalan, A. Kumar, and I. Leyva, *Chaos* **29**, 041102 (2019).
- [57] U. K. Verma and G. Ambika, *Phys. Lett. A* **450**, 128391 (2022).
- [58] S. Majhi, M. Perc, and D. Ghosh, *Chaos* **27**, 073109 (2017).
- [59] N. S. Frolov, V. A. Maksimenko, V. V. Makarov, D. V. Kirsanov, A. E. Hramov, and J. Kurths, *Phys. Rev. E* **98**, 022320 (2018).
- [60] S. Kundu, S. Majhi, and D. Ghosh, *Eur. Phys. J.: Spec. Top.* **228**, 2429 (2019).
- [61] V. A. Maksimenko, V. V. Makarov, B. K. Bera, D. Ghosh, S. K. Dana, M. V. Goremyko, N. S. Frolov, A. A. Koronovskii, and A. E. Hramov, *Phys. Rev. E* **94**, 052205 (2016).
- [62] D. V. Kasatkin and V. I. Nekorkin, *Chaos* **28**, 093115 (2018).
- [63] M. Mikhaylenko, L. Ramlow, S. Jalan, and A. Zakharova, *Chaos* **29**, 023122 (2019).
- [64] I. Omelchenko, T. Hülsler, A. Zakharova, and E. Schöll, *Front. Appl. Math. Stat.* **4**, 67 (2019).
- [65] G. Ruzzene, I. Omelchenko, J. Sawicki, A. Zakharova, E. Schöll, and R. G. Andrzejak, *Phys. Rev. E* **102**, 052216 (2020).
- [66] V. V. Semenov and A. Zakharova, *Chaos* **32**, 121106 (2022).
- [67] M. E. Yamakou, P. G. Hjorth, and E. A. Martens, *Front. Comput. Neurosci.* **14**, 62 (2020).
- [68] M. E. Yamakou and J. Jost, *Phys. Rev. E* **100**, 022313 (2019).
- [69] M. E. Yamakou, T. D. Tran, and J. Jost, *Front. Phys.* **10**, 909365 (2022).
- [70] N. Semenova and A. Zakharova, *Chaos* **28**, 051104 (2018).
- [71] M. Masoliver, C. Masoller, and A. Zakharova, *Chaos Solitons Fractals* **145**, 110666 (2021).
- [72] J. Sawicki, I. Omelchenko, A. Zakharova, and E. Schöll, *Phys. Rev. E* **98**, 062224 (2018).
- [73] D. Nikitin, I. Omelchenko, A. Zakharova, M. Avetyan, A. L. Fradkov, and E. Schöll, *Philos. Trans. R. Soc. A* **377**, 20180128 (2019).
- [74] X. Xu, D. Yu, and Z. Wang, *Physica D* **396**, 1 (2019).
- [75] X. Mao, X. Li, W. Ding, S. Wang, X. Zhou, and L. Qiao, *Appl. Math. Mech.* **42**, 441 (2021).
- [76] J. Sawicki, J. M. Koulén, and E. Schöll, *Chaos* **31**, 073131 (2021).
- [77] X. Mao, W. Ding, X. Zhou, S. Wang, and X. Li, *Electron. Res. Arch.* **29**, 2973 (2021).
- [78] K. Rajagopal, S. Panahi, Z. Shourgashti, A. Karthikeyan, and I. Hussain, *Eur. Phys. J.: Spec. Top.* **231**, 921 (2022).
- [79] W. Ding, X. Mao, L. Qiao, M. Guan, and M. Shao, *Electron. Res. Arch.* **30**, 1075 (2022).
- [80] X. Mao and F. Lei, *Int. J. Bifurcation Chaos* **32**, 2250148 (2022).
- [81] F. R. K. Chung, *Spectral Graph Theory* (American Mathematical Society, Providence, RI, 1997).
- [82] F. M. Atay, *J. Differ. Equ.* **221**, 190 (2006).
- [83] Y. Sugitani and K. Konishi, *Phys. Rev. E* **96**, 042216 (2017).
- [84] U. Kumar Verma and G. Ambika, *Front. Comput. Neurosci.* **15**, 774969 (2021).
- [85] N. Zhao, Z. Sun, X. Song, and Y. Xiao, *Physica A* **608**, 128288 (2022).
- [86] C. D. Meyer, *Matrix Analysis and Applied Linear Algebra* (SIAM, Philadelphia, PA, 2000).
- [87] D. Breda, S. Maset, and R. Vermiglio, *Stability of Linear Delay Differential Equations* (Springer, New York, NY, 2015).